

Light scattering from disordered overlayers of metallic nanoparticles

Peter Johansson

*Division of Solid State Theory, Department of Physics, University of Lund, Sölvegatan 14 A, S-223 62 Lund, Sweden
and Department of Natural Sciences, University of Örebro, S-701 82 Örebro, Sweden*

(October 31, 2018)

We develop a theory for light scattering from a disordered layer of metal nanoparticles resting on a sample. Averaging over different disorder realizations is done by a coherent potential approximation. The calculational scheme takes into account effects of retardation, multipole excitations, and interactions with the sample. We apply the theory to a system similar to the one studied experimentally by Stuart and Hall [Phys. Rev. Lett. **80**, 5663 (1998)] who used a layered Si/SiO₂/Si sample. The calculated results agree rather well with the experimental ones. In particular we find conspicuous maxima in the scattering intensity at long wavelengths (much longer than those corresponding to plasmon resonances in the particles). We show that these maxima have their origin in interference phenomena in the layered sample.

PACS numbers: 78.67.-n, 42.82.Et, 42.25.Dd

I. INTRODUCTION

During the last several years there has been an increased interest in near-field optics. This development has been driven in part by the development of the near-field scanning optical microscope, but also by a growing awareness of the importance of near-field effects and the influence they have on the radiated, far fields. Examples of probes that investigate or make use of the coupling between near-field and far-field effects include surface-enhanced Raman scattering (SERS),¹ light emission from scanning tunneling microscopes,² transmission through, and reflection from, narrow gratings,^{3,4} and scattering from particle arrays.^{5–7} Applications range from single-molecule spectroscopy using SERS to creating microcavity light sources⁸ and using the plasmon resonances of metallic nanoparticles for the transmission of “optical” signals at a sub-wavelength length scale.⁹

The optical properties of small metallic particles and collections thereof have been studied intensively both experimentally^{10–12,5–7} and theoretically.^{13–20} Many of these studies have focused on measuring and calculating properties such as average transmission and absorption in a colloidal solutions or surface films, and to determine the role of inter-particle interactions on these properties. At present there is also a lot of interest in studying the interaction between surface plasmons and particles resting on the surface in question since the presence of the particles can induce surface-plasmon band gaps.^{21,22}

In this paper we will focus on, and develop a theory for diffuse light scattering from disordered overlayers of nanoparticles resting on a sample. The motivation for this work was initially provided by an experiment in which Stuart and Hall (SH)⁵ measured the diffuse light scattering from random silver nanoparticle arrays fabricated on top of dielectric as well as semiconducting and metallic samples. The silver particles had a size of some 100 nm and the intensity of scattered light as a function of photon energy showed rather intriguing features. The

most striking result was that the scattering intensity had pronounced maxima at very long wavelengths ($\lambda > 1000$ nm) when the sample consisted of Si and SiO₂ in a multilayer structure. Stuart and Hall⁵ attributed this to an enhancement of the dipole-dipole interaction between the different particles mediated by waveguide modes that are supported by the layered sample. In this scenario, incident light is initially scattered into a waveguide mode in the sample by the nanoparticle array. The electromagnetic field associated with a waveguide mode is in general evanescent outside the sample. Therefore light scattered into such a mode is “trapped” by the sample and can travel a relatively long distance before it is damped due to losses in the sample or because it is rescattered into free space by the nanoparticles. Thus, it is clear that the presence of a sample can lead to an increase in the particle-particle interactions. Nevertheless, as we will see below, the results of this calculation do not support the scenario of Stuart and Hall.

A rigorous theory that can be used to calculate the scattering intensity from the system in question must include a number of ingredients: particle-particle interactions through near-field and far-field interactions as well as interactions mediated by the sample have to be taken into account. In addition, the nanoparticle layer is disordered and the calculation must deal with the averaging over different disorder realizations. Here we do this by means of a lattice-gas model¹⁵ in which the sites of a regular lattice are either occupied by spheres of a certain size and composition or else empty; the averaging over different realizations of the disorder is then done by a coherent potential approximation (CPA).^{23,15} In previous work, Persson and Liebsch (PL)¹⁵ dealt with a similar model within the CPA. Their treatment accounted for non-retarded dipole-dipole interactions between the particles. Later Stefanou and Modinos (SM)¹⁹ studied the same model. Their treatment of disorder effects used the simpler average T-matrix approximation (ATA), however, they did include retardation effects

as well as sample-mediated interactions in their theory. Both PL and SM concentrated on calculating the average transmission through, and reflection from arrays of relatively small particles ($R \lesssim 10$ nm). Meier, Wokaun, and Liao¹⁶ have also studied dipole-dipole interactions in a self-consistent way in a disordered array of particles by convoluting the response of a single-particle with a function describing the distribution of particles in the array.

Our theory goes beyond earlier treatments^{15,16,19} in that it simultaneously includes effects of retardation, multipolar excitations, interactions with the sample, and disorder. Moreover, since we wish to calculate the intensity of diffusely scattered light, we do not only calculate disorder-averaged fields and particle polarizabilities (which one obtains from the CPA), but also disorder-averaged intensities. We calculate these intensities within a conserving approximation, thus using an averaging procedure that includes exactly the same kind of scattering processes as the CPA calculation of the average fields. In the language of many-body theory,²⁴ evaluating the average polarizabilities is quite analogous to a single-particle self energy calculation, whereas the calculation of the diffuse scattering intensities requires that a vertex function (involving two-particle correlations) is solved for.

The calculated results show good agreement with the experimental ones. In particular, as in the experiment,⁵ a series of resonance peaks emerge in the spectrum of diffusely scattered light at relatively small photon energies. A detailed study of the behind-lying mechanisms shows that these resonances occur whenever the field that drives the plasma oscillations in the silver particles reaches a maximum. This driving field is the sum of a contribution from the incident wave and a contribution from the wave reflected from the sample. The driving field displays a number of oscillations due to interference between waves reflected from the different interfaces in the multilayered sample. Thus, the interpretation we arrive at is simpler than the one proposed by SH.⁵ It is, however, consistent with conclusions drawn from earlier experimental results by Leitner *et al.*¹² who studied light scattering from a silver island film resting on a layered sample and observed characteristic changes in the scattering spectrum as the sample geometry was varied.

The rest of the paper is organized in the following way. In Sec. II the basic theory is outlined, while Sec. III describes the theory involved in the disorder-averaging. In Sec. IV the numerical results are presented and discussed, and Sec. V gives a brief summary of the paper. Three appendices contain information on more technical aspects of the calculations.

II. BASIC THEORY

The system we consider consists of an array of spheres placed on or above a semi-infinite sample that may be lay-

ered. A schematic illustration of the system is shown in Fig. 1. The optical properties of the sample and particle materials are taken into account through local dielectric functions tabulated by Palik.²⁵ Since we will deal with relatively large particles non-local corrections to the dielectric properties should be relatively small.

To begin with we assume that the array of spheres is perfectly ordered, but later we will relax this assumption replacing the array with a lattice gas where a particular site is occupied by a sphere with probability p and unoccupied with probability $1 - p$.

A. Kirchoff integrals

The basic task before us is to calculate the electric and magnetic fields everywhere in space given an incident wave with electric field \mathbf{E}^{ext} , and magnetic field \mathbf{B}^{ext} . We will use the vector equivalents of the Kirchoff integral²⁶ to do this. These formulae read (a time-dependence $e^{-i\omega t}$ is implicitly assumed everywhere)

$$\begin{aligned} \mathbf{E}(\mathbf{r}) = & \mathbf{E}^{\text{ext}}(\mathbf{r}) + \int dS' [ikc(\hat{n}' \times \mathbf{B}(\mathbf{r}'))G(\mathbf{r}, \mathbf{r}') \\ & + (\hat{n}' \times \mathbf{E}(\mathbf{r}')) \times \nabla' G + (\hat{n}' \cdot \mathbf{E}(\mathbf{r}'))\nabla' G] \end{aligned} \quad (2.1)$$

and

$$\begin{aligned} \mathbf{B}(\mathbf{r}) = & \mathbf{B}^{\text{ext}}(\mathbf{r}) + \int dS' \left[-\frac{ik}{c}(\hat{n}' \times \mathbf{E}(\mathbf{r}'))G(\mathbf{r}, \mathbf{r}') \right. \\ & \left. + (\hat{n}' \times \mathbf{B}(\mathbf{r}')) \times \nabla' G + (\hat{n}' \cdot \mathbf{B}(\mathbf{r}'))\nabla' G \right]. \end{aligned} \quad (2.2)$$

Here G denotes the Green's function of the scalar Helmholtz equation in free space, thus G can be written

$$G(\mathbf{r}, \mathbf{r}') = \frac{e^{ik|\mathbf{r}-\mathbf{r}'|}}{4\pi|\mathbf{r}-\mathbf{r}'|} \quad (2.3)$$

and solves

$$[\nabla^2 + k^2]G(\mathbf{r}, \mathbf{r}') = -\delta^{(3)}(\mathbf{r} - \mathbf{r}'), \quad (2.4)$$

where $k = \omega/c$. The integrals appearing in Eqs. (2.1) and (2.2) run over all surfaces that enclose the nanoparticles as well as the sample, and the \mathbf{E} and \mathbf{B} fields appearing inside the integrals are the exact fields at these surfaces. Thus, Eqs. (2.1) and (2.2) are coupled integral equations from which the electromagnetic field always, at least in principle, can be calculated.

The Kirchoff integrals become very useful also for detailed calculations once we have analytic expressions for the fields inside the spheres in the array and in the sample. In the rest of this section, however, they will mainly be used as a tool to aid our thinking.

B. Multipole fields and sphere response

The electromagnetic field inside and around each sphere can be expressed in terms of electric (\mathbf{E}) and magnetic (\mathbf{M}) multipole fields. An *electric* multipole field is defined by (we use Jackson's definitions²⁶)

$$\mathbf{B}^{(E)} = \frac{k}{c} z_l(k_r r) \mathbf{X}_{lm}; \quad \mathbf{E}^{(E)} = \frac{i}{\epsilon_r} \nabla \times [z_l(k_r r) \mathbf{X}_{lm}], \quad (2.5)$$

where k_r is the magnitude of the wave vector $k_r = \sqrt{\epsilon_r} \omega / c$ in a material with relative dielectric function ϵ_r .²⁵ A *magnetic* multipole is associated with the fields

$$\mathbf{E}^{(M)} = k z_l(k_r r) \mathbf{X}_{lm}; \quad \mathbf{B}^{(M)} = -\frac{i}{c} \nabla \times [z_l(k_r r) \mathbf{X}_{lm}]. \quad (2.6)$$

In both these equations the vector spherical harmonic

$$\mathbf{X}_{lm} = (\mathbf{L} Y_{lm}) / \sqrt{l(l+1)}. \quad (2.7)$$

is defined in terms of the angular momentum operator $\mathbf{L} \equiv -i\mathbf{r} \times \nabla$ and the usual spherical harmonics Y_{lm} . The vector spherical harmonics fulfill the orthogonality relations $\int d\Omega \mathbf{X}_{l'm'}^*(\Omega) \cdot \mathbf{X}_{lm}(\Omega) = \delta_{ll'} \delta_{mm'}$, and $\int d\Omega \mathbf{X}_{l'm'}^*(\Omega) \cdot [\hat{\mathbf{r}} \times \mathbf{X}_{lm}(\Omega)] = 0$ on the unit sphere. The function $z_l(k_r r)$ stands for a linear combination of a spherical Bessel function $j_l(k_r r)$, which is regular at $r = 0$, and a spherical Hankel function of the first kind $h_l(k_r r) = j_l(k_r r) + in_l(k_r r)$, which describes outgoing waves.

In the present case, we can write the electric field inside the sphere at site i as

$$\mathbf{E} = \sum_{lm} k c_{lm}^{(M)} j_l(k_r r) \mathbf{X}_{lm} + \frac{i}{\epsilon_r} \nabla \times \left[c_{lm}^{(E)} j_l(k_r r) \mathbf{X}_{lm} \right]. \quad (2.8)$$

Since the fields must be defined at the sphere center, only Bessel functions j_l appear. Just outside the sphere, we have instead

$$\mathbf{E} = \sum_{lm} k [a_{lm}^{(M)} j_l(kr) + b_{lm}^{(M)} h_l(kr)] \mathbf{X}_{lm} + i \nabla \times \left\{ [a_{lm}^{(E)} j_l(kr) + b_{lm}^{(E)} h_l(kr)] \mathbf{X}_{lm} \right\}. \quad (2.9)$$

Demanding that the usual boundary conditions for the \mathbf{E} and \mathbf{B} fields are satisfied at the surface of the sphere one can derive equations from which the field inside a sphere (the c coefficient) and the scattered field (b coefficient) can be calculated for each multipole, given the incident field (a coefficient). Since we focus on scattering properties, the key quantities are the ‘‘sphere-response functions’’

$$s_l^{(E)} = \frac{b_{lm}^{(E)}}{a_{lm}^{(E)}} = -\frac{\epsilon k R j_l'(kR) + j_l(kR) (\epsilon - 1 - \mathcal{J}_l)}{\epsilon k R h_l'(kR) + h_l(kR) (\epsilon - 1 - \mathcal{J}_l)}, \quad (2.10)$$

and

$$s_l^{(M)} = \frac{b_{lm}^{(M)}}{a_{lm}^{(M)}} = -\frac{k R j_l'(kR) - j_l(kR) \mathcal{J}_l}{k R h_l'(kR) - h_l(kR) \mathcal{J}_l}, \quad (2.11)$$

where \mathcal{J}_l is shorthand for

$$\mathcal{J}_l = k_r R j_l'(k_r R) / j_l(k_r R).$$

Thanks to the symmetry of the sphere these response functions are independent of m .

In the following, we will often describe the ‘‘state’’ of a sphere through the a and b coefficients. It is therefore convenient to collect these coefficients into vectors \vec{a}_i and \vec{b}_i in ‘‘multipole space’’ with the structure

$$\vec{a}_i = \left(a_{1-1,i}^{(E)}; a_{10,i}^{(E)}; \dots; a_{l_{max} l_{max},i}^{(E)}; a_{1-1,i}^{(M)}; \dots; a_{l_{max} l_{max},i}^{(M)} \right), \quad (2.12)$$

etc.²⁷ If we form a diagonal tensor \overleftrightarrow{s} , in which the response functions $s_{lm}^{(E)}$ and $s_{lm}^{(M)}$ enter in the appropriate places, the relation between incoming and outgoing waves at site i can be written

$$\vec{b}_i = \overleftrightarrow{s} \vec{a}_i. \quad (2.13)$$

C. Surface response

Light will be scattered also from the sample surface and we need to deal with the surface response. A plane wave incident on the sample surface has a wave vector

$$\mathbf{q}_- = \mathbf{q}_\parallel - \hat{z} \sqrt{k^2 - |\mathbf{q}_\parallel|^2} \quad (2.14)$$

(the subscript ‘‘-’’ indicates that the wave propagates in the negative z direction) and can be written

$$\mathbf{E} = \left\{ E^{(s)} \hat{s} + E^{(p)} \hat{p} \right\} e^{i\mathbf{q}_- \cdot \mathbf{r}} \quad (2.15)$$

where the unit vectors for s and p polarization are $\hat{s} = [\hat{z} \times \hat{q}_\parallel]$ and $\hat{p} = -[\hat{q}_- \times (\hat{z} \times \hat{q}_\parallel)]$, respectively. Here \hat{q}_- is a unit vector in the direction of the wave vector, and \hat{q}_\parallel is a unit vector in the direction of the in-plane component of the wave vector.

The reflected wave in response to the incident one (2.15) can be written

$$\mathbf{E}_{\text{refl}} = \left\{ \chi_s(\mathbf{q}_\parallel, \omega) E^{(s)} \hat{s} + \chi_p(\mathbf{q}_\parallel, \omega) E^{(p)} \hat{p} \right\} e^{i\mathbf{q}_+ \cdot \mathbf{r}}, \quad (2.16)$$

where now $\mathbf{q}_+ = \mathbf{q}_\parallel + \hat{z}\sqrt{k^2 - |\mathbf{q}_\parallel|^2}$ and $\hat{p} = -[\hat{q}_+ \times (\hat{z} \times \hat{q}_\parallel)]$ for this wave vector. In case the sample is *homogeneous* the surface response functions χ_s and χ_p are found from the Fresnel formulae yielding

$$\chi_s(\mathbf{q}_\parallel, \omega) = \frac{\sqrt{k^2 - \mathbf{q}_\parallel^2} - \sqrt{k_s^2 - \mathbf{q}_\parallel^2}}{\sqrt{k^2 - \mathbf{q}_\parallel^2} + \sqrt{k_s^2 - \mathbf{q}_\parallel^2}}, \quad (2.17)$$

where k_s is the wave number in the sample depending on the dielectric function of the sample $\epsilon_s(\omega)$,

$$k_s^2 = \epsilon_s(\omega)k^2.$$

For p polarized light one gets

$$\chi_p(\mathbf{q}_\parallel, \omega) = \frac{\epsilon_s \sqrt{k^2 - \mathbf{q}_\parallel^2} - \sqrt{k_s^2 - \mathbf{q}_\parallel^2}}{\epsilon_s \sqrt{k^2 - \mathbf{q}_\parallel^2} + \sqrt{k_s^2 - \mathbf{q}_\parallel^2}}. \quad (2.18)$$

Note that the expressions for all the surface response functions can be extended to the case of evanescent waves for which $|\mathbf{q}_\parallel| > k$ (when evaluating square roots the branch cut lies below the positive real axis). For lack of a better terminology, “plane wave” will sometimes be used to describe both propagating plane waves and waves that propagate in the directions parallel to the sample surface but are evanescent in the third, z , direction.

When the sample consists of several layers of different materials the response functions χ_p and χ_s must be calculated by a generalized approach, for example a transfer matrix formalism, see Ref. 28. Then one first makes an Ansatz for the electromagnetic field in the bottom layer of the sample in terms of one plane wave that propagates or decays exponentially in the downward direction. Then this wave is matched to a downgoing and an upgoing wave at the bottom interface. These waves are propagated through the next layer, matched at the next interface, etc., until one reaches the sample surface where the ratio between the incident and upgoing wave amplitudes yields the surface response for the two different polarization types.

D. Multiple-scattering solution for an ordered array

Having introduced the necessary basic ingredients of the calculation we consider now the complete array of spheres (without the sample for the moment), and let a plane wave like the one in Eq. (2.15) impinge on this system. Now Eq. (2.13) can be written

$$\vec{b}_i = \overset{\leftrightarrow}{s} \left[\vec{a}_i^{\text{dir}} + \sum_{j \neq i} \overset{\leftrightarrow}{t}_{ij}^{\text{dir}} \vec{b}_j \right]. \quad (2.19)$$

Thus the incident field at sphere i is, as can be understood by looking at Eqs. (2.1) and (2.2), a sum of one contribution, \vec{a}_i^{dir} , coming from the projection of the plane

wave in Eq. (2.15) onto the various multipoles, and contributions from waves scattered off all the other spheres. The explicit, rather lengthy, expressions for \vec{a}_i^{dir} and the coupling coefficients t_{ij}^{dir} (or rather its Fourier transform) are derived in Appendices A and B, respectively.

Thanks to the periodicity of the sphere array, $\overset{\leftrightarrow}{t}_{ij}$ only depends on the relative vector $\mathbf{R}_i - \mathbf{R}_j$ separating spheres i and j , and Eq. (2.19) can be solved by a Fourier transformation. For an arbitrary quantity Z defined on the lattice we introduce the Fourier transform

$$Z_{\mathbf{Q}} = \sum_i Z_i e^{-i\mathbf{Q} \cdot \mathbf{R}_i}, \quad (2.20)$$

and its inverse

$$Z_i = \frac{1}{N} \sum_{\mathbf{Q}} Z_{\mathbf{Q}} e^{i\mathbf{Q} \cdot \mathbf{R}_i}, \quad (2.21)$$

where N is the number of lattice sites. Applied to Eq. (2.19) this yields

$$\vec{b}_{\mathbf{Q}} = \overset{\leftrightarrow}{s} \left[\vec{a}_{\mathbf{Q}}^{\text{dir}} + \overset{\leftrightarrow}{t}_{\mathbf{Q}}^{\text{dir}} \vec{b}_{\mathbf{Q}} \right], \quad (2.22)$$

so that

$$\vec{b}_{\mathbf{Q}} = \left[\overset{\leftrightarrow}{1} - \overset{\leftrightarrow}{s} \overset{\leftrightarrow}{t}_{\mathbf{Q}}^{\text{dir}} \right]^{-1} \overset{\leftrightarrow}{s} \vec{a}_{\mathbf{Q}}^{\text{dir}}. \quad (2.23)$$

When the sample is added to the problem one more surface, the plane $z = z_0 = -R$, will contribute to the Kirchoff integrals. The waves that are sent out from the sample surface are in turn emitted in response to the incident plane wave or waves coming from the spheres. Consequently Eq. (2.13) now reads

$$\vec{b}_i = \overset{\leftrightarrow}{s} \left[\vec{a}_i^{\text{dir}} + \vec{a}_i^{\text{ref}} + \overset{\leftrightarrow}{w} \vec{b}_i + \sum_{j \neq i} (\overset{\leftrightarrow}{t}_{ij}^{\text{dir}} + \overset{\leftrightarrow}{t}_{ij}^{\text{sub}}) \vec{b}_j \right], \quad (2.24)$$

where \vec{a}_i^{ref} is the contribution from the incident wave after it has been reflected *once* from the sample, $\overset{\leftrightarrow}{w}$ is the sample-mediated self-interaction between the various multipoles on a sphere, while $\overset{\leftrightarrow}{t}^{\text{sub}}$ is the sample-mediated interaction between two different spheres. These quantities are discussed in Appendix C. It should be kept in mind that both $\overset{\leftrightarrow}{w}$ and $\overset{\leftrightarrow}{t}^{\text{sub}}$ describe events in which the source sphere sends out a wave that is scattered once off the sample and then goes directly to the receiving sphere; multiple scattering events enter through Eq. (2.24). We introduce a total driving field

$$\vec{a}_i^{\text{ext}} = \vec{a}_i^{\text{dir}} + \vec{a}_i^{\text{ref}}, \quad (2.25)$$

and a total sphere-sphere interaction

$$\overset{\leftrightarrow}{t}_{ij} = \overset{\leftrightarrow}{t}_{ij}^{\text{dir}} + \overset{\leftrightarrow}{t}_{ij}^{\text{sub}}, \quad (2.26)$$

and Fourier-transforming we find the solution for $\vec{b}_{\mathbf{Q}}$

$$\vec{b}_{\mathbf{Q}} = \left[\vec{1} - \overleftrightarrow{s}\overleftrightarrow{w} - \overleftrightarrow{s}\overleftrightarrow{t}_{\mathbf{Q}} \right]^{-1} \overleftrightarrow{s}\vec{a}_{\mathbf{Q}}^{\text{ext}}. \quad (2.27)$$

It is also possible to rewrite Eq. (2.24) as

$$\vec{b}_i = (\vec{1} - \overleftrightarrow{s}\overleftrightarrow{w})^{-1} \overleftrightarrow{s} \left[\vec{a}_i^{\text{ext}} + \sum_{j \neq i} \overleftrightarrow{t}_{ij} \vec{b}_j \right]. \quad (2.28)$$

Thus, the sample-mediated self-interaction does not appear explicitly in this equation, but is instead accounted for by the modified response tensor $(\vec{1} - \overleftrightarrow{s}\overleftrightarrow{w})^{-1} \overleftrightarrow{s}$. Interparticle interactions mediated by the sample are of course still included in $\overleftrightarrow{t}_{ij}$. The reasoning behind Eq. (2.28) in many ways makes it easier to think of the problem, since the sample in a sense has been eliminated from the formalism. The effects of the sample on the spheres are summarized by the modification of the response tensor and the additional contribution $\overleftrightarrow{t}_{ij}^{\text{sub}}$ to the particle-particle interaction.

III. DISORDERED ARRAY

A. Coherent potential approximation

In the previous section we dealt with a system where each site on the lattice was occupied by a sphere. We will now treat a disorder model, namely a lattice gas. We still have a square lattice but only a random fraction p of the sites are occupied by spheres, whereas the rest of the sites are empty.

The averaging over different disorder realizations will be done within the coherent-potential approximation.²³ The CPA is known to be the best single-site mean-field theory, and it gives correct results in a number of important limits. A certain realization of the disordered system is characterized by the response function of the sphere occupying the various sites; at the empty sites this response (\overleftrightarrow{s}) vanishes. Within the CPA calculation we aim at finding an effective medium in which *every* site is occupied by average objects that can also be described by a surface response tensor that we will denote $\overleftrightarrow{\alpha}$ in the following. As we saw above, the treatment can be simplified by incorporating the sample-mediated self interaction into the particle response. For the average particles we do this by also introducing the tensor $\overleftrightarrow{\beta}$ which is related to $\overleftrightarrow{\alpha}$ by

$$\overleftrightarrow{\beta} = (\vec{1} - \overleftrightarrow{\alpha}\overleftrightarrow{w})^{-1} \overleftrightarrow{\alpha}, \quad \Leftrightarrow \quad \overleftrightarrow{\alpha} = (\vec{1} + \overleftrightarrow{\beta}\overleftrightarrow{w})^{-1} \overleftrightarrow{\beta}. \quad (3.1)$$

It should already now be pointed out that the tensors $\overleftrightarrow{\alpha}$ and $\overleftrightarrow{\beta}$, describing the average scatterers, are not diagonal; the spherical symmetry is lost when interactions with the environment are taken into account. For example, in the case that the particles are treated as dipoles, the average particles have different polarizabilities in the directions parallel to, and normal to the plane

of the array, respectively.¹⁵ Both $\overleftrightarrow{\alpha}$ and $\overleftrightarrow{\beta}$ are, however, still lattice symmetric. Thus, only those tensor elements that couple multipoles belonging to the same irreducible representation of the array point group (in the present case where the particles interact with a sample, C_{4v}) are nonzero.

The response functions $\overleftrightarrow{\alpha}$ and $\overleftrightarrow{\beta}$ are determined self-consistently by placing a real site, i.e. one which is occupied by a real sphere with probability p and empty with probability $1 - p$ in the effective medium of average particles, and demanding that the real site does not cause any additional scattering on the average.

To see what this means in detail, we consider the scattering off the real site as compared with when it is occupied by an average scatterer. An occupied real site yields the *extra* outgoing waves

$$\vec{b}_{1,\text{extra}} = (\overleftrightarrow{\beta}_{\text{oc}} - \overleftrightarrow{\beta}) \vec{a}_0 \quad (3.2)$$

in a *single scattering event*. In Eq. (3.2)

$$\overleftrightarrow{\beta}_{\text{oc}} = (\vec{1} - \overleftrightarrow{s}\overleftrightarrow{w})^{-1} \overleftrightarrow{s}, \quad (3.3)$$

the effective response function for a real sphere including the sample-mediated self interaction, and \vec{a}_0 could describe any combination of waves incident on the real site. In the CPA one includes not only single scattering events off the real site, but takes into account multiple scattering to all orders. This means that the extra scattering from an occupied site can be written with the aid of a T matrix $\overleftrightarrow{T}_{\text{oc}}$,

$$\vec{b}_{\text{oc,extra}} = \overleftrightarrow{T}_{\text{oc}} \vec{a}_0 = \left[\vec{1} - (\overleftrightarrow{\beta}_{\text{oc}} - \overleftrightarrow{\beta}) \overleftrightarrow{\gamma}_{00} \right]^{-1} (\overleftrightarrow{\beta}_{\text{oc}} - \overleftrightarrow{\beta}) \vec{a}_0. \quad (3.4)$$

Here $\overleftrightarrow{\gamma}_{00}$ is a propagator for multipole excitations describing how waves sent out from the real site propagate through the effective medium of average scatterers and eventually return to the real, central site. One can show that

$$\overleftrightarrow{\gamma}_{00} = N^{-1} \sum_{\mathbf{Q}} \left(\vec{1} - \overleftrightarrow{t}_{\mathbf{Q}} \overleftrightarrow{\beta} \right)^{-1} \overleftrightarrow{t}_{\mathbf{Q}}. \quad (3.5)$$

If instead the real site is empty, the extra scattering can be written

$$\vec{b}_{\text{un,extra}} = \overleftrightarrow{T}_{\text{un}} \vec{a}_0 = \left[\vec{1} - (\overleftrightarrow{\beta}_{\text{un}} - \overleftrightarrow{\beta}) \overleftrightarrow{\gamma}_{00} \right]^{-1} (\overleftrightarrow{\beta}_{\text{un}} - \overleftrightarrow{\beta}) \vec{a}_0. \quad (3.6)$$

Of course in this case the empty site does not give any scattering, i.e. $\overleftrightarrow{\beta}_{\text{un}} = \vec{0}$, and

$$\vec{b}_{\text{un,extra}} = \left[\vec{1} + \overleftrightarrow{\beta} \overleftrightarrow{\gamma}_{00} \right]^{-1} (-\overleftrightarrow{\beta}) \vec{a}_0. \quad (3.7)$$

The CPA self-consistency condition demanding that there should be *no extra scattering on the average* means that

$$p \vec{b}_{oc,extra} + (1-p) \vec{b}_{un,extra} = 0. \quad (3.8)$$

After some algebra Eq. (3.8) can be rewritten as

$$\vec{\beta} = p \vec{\beta}_{oc} \left\{ \vec{1} + \vec{\gamma}_{00} \left[\vec{\beta} - \vec{\beta}_{oc} \right] \right\}^{-1}. \quad (3.9)$$

Equation (3.9) has to be solved for $\vec{\beta}$ by an iterative process in which also $\vec{\gamma}_{00}$ in Eq. (3.5) has to be updated in each step of the iteration.

From Eq. (3.9) it is easy to verify one of the celebrated features of the CPA, namely that it approaches the correct limit for both $p = 0$ when $\vec{\beta} = 0$, and $p = 1$ for which the self-consistent solution is $\vec{\beta} = \vec{\beta}_{oc} = (\vec{1} - \vec{s}\vec{w})^{-1}\vec{s}$.

B. Diffuse scattering

So far we have found the response functions $\vec{\alpha}$ and $\vec{\beta}$ that characterize an average effective medium that has the same effect as the lattice gas of particles on the incident light in terms of *coherent* transmission and reflection.

To calculate the intensity of diffusely scattered light into a certain direction, the theory has to be developed further. Up to now we have only calculated average quantities involving one single multipole excitation, but to find diffuse scattering *intensities* averages involving two multipole excitations must be calculated.

Suppose that a plane wave described by the amplitude vector $\vec{a}_{\mathbf{Q}}^{\text{ext}}$ impinges on the disordered particle array. In response to this there will of course be multipole excitations at the incident wave vector \mathbf{Q} that can be characterized by $\vec{b}_{\mathbf{Q}}$. But as a result of the disorder there are also multipole excitations described by $\vec{b}_{\mathbf{Q}'}$ at other wave vectors \mathbf{Q}' . Now, averaging over a large number of different disorder realizations (in our case, lattice gas arrangements) would show that $\langle \vec{b}_{\mathbf{Q}} \rangle \neq 0$, (here $\langle X \rangle$ denotes disorder-averaging of the quantity X) whereas $\langle \vec{b}_{\mathbf{Q}'} \rangle = 0$, since the diffusely scattered light has an essentially random phase that varies from one disorder realization to another. Yet averages like $\langle b_{\xi, \mathbf{Q}'}^* b_{\zeta, \mathbf{Q}'} \rangle$ (ξ and ζ are shorthand indices for different multipoles) of course do *not* vanish and hence there is diffusely scattered light.

Assume that we have managed to calculate the coefficients $\vec{b}_{\zeta \mathbf{Q}'}$ for one particular realization of the disorder. The (reflected) scattered electric field $\mathbf{E}_{sc}(\mathbf{r})$, with a wave vector

$$\mathbf{q}' = \mathbf{q}'_{\parallel} + q'_z \hat{z} \quad \text{with} \quad q'_z = \sqrt{k^2 - q'_{\parallel}{}^2}$$

whose in-plane wave vector $\mathbf{q}'_{\parallel} = \mathbf{Q}' + \mathbf{G}$ equals \mathbf{Q}' up to a reciprocal lattice vector $\mathbf{G} = (2\pi/a)(n_x \hat{x} + n_y \hat{y})$ with n_x and n_y being integers, can then be written

$$\mathbf{E}_{sc}(\mathbf{r}) = \int \frac{d^2 q'_{\parallel}}{(2\pi)^2} \sum_{\zeta} b_{\zeta \mathbf{Q}'} \left[\hat{s} d_{\zeta}^s(\mathbf{q}') + \hat{p} d_{\zeta}^p(\mathbf{q}') \right]. \quad (3.10)$$

Here the function

$$d_{\zeta}^s(\mathbf{q}') = g_{\zeta}^s(\mathbf{q}'_+) + e^{2i\sqrt{k^2 - q'_{\parallel}{}^2}|z_0|} \chi_s(\mathbf{q}'_{\parallel}) g_{\zeta}^s(\mathbf{q}'_-) \quad (3.11)$$

describes coupling from multipole ζ to an outgoing s polarized wave, either directly (first term) or through a reflection off the sample (second term). The functions $g_{\zeta}^{s,p}$ which are defined in Appendix A, measure the “overlap” between multipole ζ and a plane wave with wave vector $\mathbf{q}'_{\pm} = \mathbf{q}'_{\parallel} \pm q'_z \hat{z}$. When the wave leaves the system without being reflected off the sample the wave vector should have a positive z component, whereas when a reflection takes place the multipole must first couple to a down-going plane wave (\mathbf{q}'_-), and the amplitude of the wave is also affected by a phase shift due to the additional distance that the wave must travel and the surface response function χ_s . In the same way,

$$d_{\zeta}^p(\mathbf{q}') = g_{\zeta}^p(\mathbf{q}'_+) + e^{2i\sqrt{k^2 - q'_{\parallel}{}^2}|z_0|} \chi_p(\mathbf{q}'_{\parallel}) g_{\zeta}^p(\mathbf{q}'_-) \quad (3.12)$$

for outgoing p polarized waves. The scattered power is now for this particular realization

$$P_{sc} = \frac{c \epsilon_0}{2} \int \frac{d^2 q'_{\parallel}}{(2\pi)^2} \sum_{\xi \zeta} b_{\xi \mathbf{Q}'}^* b_{\zeta \mathbf{Q}'} \times \left[d_{\xi}^s(\mathbf{q}')^* d_{\zeta}^s(\mathbf{q}') + d_{\xi}^p(\mathbf{q}')^* d_{\zeta}^p(\mathbf{q}') \right]. \quad (3.13)$$

If we were to calculate the scattered power for *another* realization of the disorder we would arrive at the same formal expression (3.13); the functions $d_{\xi}^{s(p)}(\mathbf{q}')$ would still be the same, however, the values of the b coefficients would of course be different. Thus, the disorder-averaged scattered power is given by Eq. (3.13) provided that the product $b_{\xi \mathbf{Q}'}^* b_{\zeta \mathbf{Q}'}$ is replaced by its disorder-average

$$b_{\xi \mathbf{Q}'}^* b_{\zeta \mathbf{Q}'} \rightarrow \langle b_{\xi \mathbf{Q}'}^* b_{\zeta \mathbf{Q}'} \rangle.$$

Obviously, to find the intensity of diffusely scattered light we must calculate the averages $\langle b_{\xi \mathbf{Q}'}^* b_{\zeta \mathbf{Q}'} \rangle$.

C. Vertex function

Since we have calculated the properties (essentially $\vec{\beta}$) of the average objects within the CPA, also the calculation of $\langle b_{\xi \mathbf{Q}'}^* b_{\zeta \mathbf{Q}'} \rangle$ must be done at the same level of approximation in order to conserve the total energy. This means that this calculation must take into account repeated single-site scattering events to all orders. To this end we have to solve a Bethe-Salpeter equation for a vertex function Λ that sums all “ladder diagrams” as illustrated in Fig. 2.²⁴

The irreducible vertex Ξ describes the simplest scattering event, off one real site, that enters the sum of ladder diagrams. It is given by an average between the scattering intensity from an occupied site and from an unoccupied site, and can be expressed in terms of the previously introduced T matrices [see Eqs. (3.4) and (3.6)] as

$$\Xi_{\zeta\delta}^{\xi\eta} = p (\overleftrightarrow{T}_{oc}^*)_{\xi\eta} (\overleftrightarrow{T}_{oc})_{\zeta\delta} + (1-p) (\overleftrightarrow{T}_{un}^*)_{\xi\eta} (\overleftrightarrow{T}_{un})_{\zeta\delta}. \quad (3.14)$$

The full vertex function Λ is then found by allowing for the possibility of consecutive scattering events off different sites. Summed to all orders this yields the Bethe-Salpeter equation (summation over repeated indices is assumed implicitly)

$$\Lambda_{\zeta\delta}^{\xi\eta} = \Xi_{\zeta\delta}^{\xi\eta} + \Xi_{\zeta\delta'}^{\xi\eta'} \Pi_{\delta'\delta''}^{\eta'\eta''} \Lambda_{\delta''\delta}^{\eta''\eta}. \quad (3.15)$$

In Eq. (3.15), Π describes the propagation of the multipole excitations through the effective medium from one scattering site to the next. This propagator involves essentially the same quantities as did the “return” propagator $\overleftrightarrow{\gamma}_{00}$ encountered earlier. We can write

$$\Pi_{\zeta\delta}^{\xi\eta} = -(\overleftrightarrow{\gamma}_{00})_{\xi\eta}^* (\overleftrightarrow{\gamma}_{00})_{\zeta\delta} + N^{-1} \sum_{\mathbf{Q}} (\overleftrightarrow{\gamma}_{\mathbf{Q}}^*)_{\xi\eta} (\overleftrightarrow{\gamma}_{\mathbf{Q}})_{\zeta\delta}, \quad (3.16)$$

where

$$\overleftrightarrow{\gamma}_{\mathbf{Q}} = \left(\overleftrightarrow{\mathbb{1}} - \overleftrightarrow{t}_{\mathbf{Q}} \overleftrightarrow{\beta} \right)^{-1} \overleftrightarrow{t}_{\mathbf{Q}}. \quad (3.17)$$

Inserting the above expressions for Ξ and Π into Eq. (3.15) we can solve for Λ numerically by means of a matrix inversion.

Finally, we must relate the vertex function to the averages $\langle b_{\xi\mathbf{Q}}^* b_{\zeta\mathbf{Q}'} \rangle$ needed to find the diffuse scattering intensity. One can write

$$\begin{aligned} \langle b_{\mathbf{Q}'\xi}^* b_{\mathbf{Q}\zeta} \rangle &= \left[\left(\overleftrightarrow{\mathbb{1}} - \overleftrightarrow{\beta} \overleftrightarrow{t}_{\mathbf{Q}'} \right)^{-1} \right]_{\xi\xi'}^* \left[\left(\overleftrightarrow{\mathbb{1}} - \overleftrightarrow{\beta} \overleftrightarrow{t}_{\mathbf{Q}} \right)^{-1} \right]_{\zeta\zeta'} \\ &\quad \times \Lambda_{\zeta'\delta}^{\xi'\eta} (\overleftrightarrow{a}^{\text{eff}*})_{\eta} (\overleftrightarrow{a}^{\text{eff}})_{\delta}. \end{aligned} \quad (3.18)$$

Here

$$\overleftrightarrow{a}^{\text{eff}} = N^{-1} \sum_{\mathbf{Q}} \left(\overleftrightarrow{\mathbb{1}} - \overleftrightarrow{t}_{\mathbf{Q}} \overleftrightarrow{\beta} \right)^{-1} \overleftrightarrow{a}_{\mathbf{Q}}^{\text{ext}} \quad (3.19)$$

represents the effective driving field at the site where the first scattering event occurs. This effective field results from screening of the external field (given by $\overleftrightarrow{a}_{\mathbf{Q}}^{\text{ext}}$) by the average particles in the effective medium. In the same way, the tensor $\left(\overleftrightarrow{\mathbb{1}} - \overleftrightarrow{\beta} \overleftrightarrow{t}_{\mathbf{Q}} \right)^{-1}$ appearing in front of Λ in Eq. (3.18) accounts for the screening of the outgoing waves by the average particles after the last scattering event has occurred. One should note that the outgoing wave vector \mathbf{Q}' occurs in this expression, whereas, in the case of an incident plane wave, there is only one term (at wave vector \mathbf{Q}) in the sum defining $\overleftrightarrow{a}^{\text{eff}}$.

IV. RESULTS AND DISCUSSION

Let us consider a system of spheres with radius $R = 50$ nm and lattice parameter $a = 120$ nm. These values probably describe the average properties of the particle overlayers studied by Stuart and Hall⁵ rather well. However, one should keep in mind that in that experiment the typical particle shape was most likely not spherical. Judging from the manufacturing process, the particles studied in that experiment looked more like oblate spheroids than spheres.

Figure 3 shows calculated results for the intensity of scattered light from a disordered array of silver particles placed on a Si/SiO₂/Si sample. In close agreement with the experimental results found in Ref. 5 the scattering intensity in Fig. 3 (a) has two isolated peaks at 1180 and 710 nm.²⁹ These isolated peaks are then followed by a broader “scattering band” at shorter wavelengths $\lesssim 550$ nm. We also note that the overall intensity of the scattered light is in reasonable agreement with the experimental results; the measured diffuse scattering intensity collected over a solid angle of $\approx 2\pi/5$ was about 1 % of the incident intensity, while we here get intensities of the order of 10 % when calculating the light collected over a solid angle of 2π .

What mechanism makes the two isolated, long-wavelength peaks appear in the spectrum? These features only appear when there is a layered sample; as can also be seen in Fig. 3 (a) there are no such peaks in the spectrum calculated with a homogeneous dielectric sample (LiF). Stuart and Hall⁵ argued that the intensity of the scattered light reaches a maximum whenever the particle-particle interaction mediated by waveguide modes in the sample reaches a maximum. While this certainly is an interesting suggestion the results of our calculation show that the isolated resonances have a simpler explanation.

The isolated peaks in the scattering intensity coincide with maxima in the electric field that polarizes the metallic particles in the first place. The dotted curve in Fig. 3(a) shows the squared strength of the driving electric field found in the plane of the sphere centers as a result of the incident wave and its reflection off the sample. This field has been calculated in the absence of the particle overlayer. In the present situation, when the incident field hits the sample at normal incidence (no physical difference between s and p polarization), the driving field can be written

$$\mathbf{E}_{\text{drive}} = E^{(s)} \hat{s} [1 + e^{2ik|z_0|} \chi_s(\mathbf{q}_{\parallel} = 0, \omega)], \quad (4.1)$$

thus the quantity plotted together with the scattering intensity in Fig. 3 is

$$\left| 1 + e^{2ik|z_0|} \chi_s(\mathbf{q}_{\parallel} = 0, \omega) \right|^2.$$

The oscillations in the driving field strength with varying wavelength is consequently a result of constructive and

destructive interference between waves reflected from different interfaces of the multilayer sample. For the case shown in Fig. 3 (a), even if the presence of the other layers also affects the driving field, the thickness d_1 , of the top Si layer is the most important parameter in determining the interference maxima and minima; $\lambda_{\text{Si}} = \lambda/\sqrt{\epsilon_{\text{Si}}}$ equals $2d_1$ when $\hbar\omega \approx 1.1$ eV ($\lambda \approx 1130$ nm), and $4d_1$ when $\hbar\omega \approx 1.9$ eV ($\lambda \approx 650$ nm). Of course, when one changes the sample geometry i.e. the thicknesses or the composition of the various layers, the maxima of the driving field shift in frequency. As can be seen in Fig. 3 (b), where the thickness d_1 of the top Si layer was increased to 240 nm, this brings with it identical shifts of the isolated peaks in the scattered intensity. This further supports the interpretation given here.

Figure 4 shows how the in-plane electric field varies with z in the Si/SiO₂/Si sample used for the calculations in Fig. 3 (a) when there is no particle overlayer and waves with photon energies 1.1 eV, 1.3 eV, 1.5 eV, and 1.7 eV, respectively, impinge on the surface at normal incidence. As can be seen there are reflection resonances when it is possible to fit in a wave that has antinodes at the interfaces of the top Si layer.

A simple explanation for why surface waveguide modes are *not* causing the scattering resonances lies in the very small scattering cross section for a single sphere at the relevant wavelengths. This cross section is of the order $(kR)^4 R^2$. With a wavelength of 1000 nm and $R = 50$ nm $kR \sim 0.3$, which means that the scattering cross section is of the order of 1 % of the geometric cross section. Now, the process discussed by Stuart and Hall⁵ involves *two* scattering events off nanoparticles because the incoming light must first be scattered into a waveguide mode by the particles and then out again in order to be observed as diffusely scattered light. Of course such a process will not be very effective, unless some other factor compensates for the small scattering cross sections. In this case the waveguide modes do offer some compensation; the response of the semiconductor surface is very strongly enhanced for combinations of in-plane wave vector \mathbf{q}_{\parallel} and photon energy $\hbar\omega$ that coincide with those of a waveguide mode. But this only happens for a narrow interval of wave vectors. There is not enough phase space for the waveguide-mode-mediated particle-particle interaction to become an important factor for the scattering of long-wavelength light.

This point is best illustrated by looking at a plot of the particle-particle interaction as a function of in-plane wave vector shown in Fig. 5. The curves show the value of $|\beta_{11,11\mathbf{Q}} t_{11,11\mathbf{Q}}|$ as a function of \mathbf{Q} for two different photon energies. This quantity yields the ratio between the secondary wave hitting a sphere as a result of a previous scattering event off the other average particles, and the primary incident wave. With this particular choice of tensor elements we are focusing the attention to the waves sent out by in-plane electric dipoles on the particles. We note that for most wave vectors the sphere-sphere coupling for these photon energies lie well below 1,

i.e. the primary wave dominates in strength over rescat-tered secondary waves. For certain wave vectors the sphere-sphere coupling is, however, rather strong. This happens when the electromagnetic oscillations of a particle are in resonance with a waveguide mode of the sample. In this case the sample-mediated coupling has a sharp peak. With $\hbar\omega = 1.0$ eV there are two such resonances. The peak marked A' is due to an s polarized waveguide mode whereas the peak B' is caused by a p polarized mode. When increasing the photon energy these peaks move out towards higher \mathbf{Q} . At 1.3 eV their corresponding positions are given by the peaks A and B. The new peak C is associated with a standing wave resonance very similar to the one occurring at $\mathbf{Q} = 0$ at 1 eV.

In this context we should also say that the waveguide modes may play a much more pronounced role in experiments with periodically ordered arrays of nanoparticles. In this case the surface modes that can be excited must have an in-plane wave vector that either equals the incident one or else differs from it by a reciprocal wave vector \mathbf{G} . In that case the sample-mediated particle-particle interaction is not averaged over different wave vectors in the same way as in the present case. The recent experiment by Linden *et al.*⁷ who measured light transmission through a layered sample covered by an array of gold nanoparticles, provides such an example.

Turning to the range of the spectrum at higher photon energies, the features appearing there are caused by a combination of particle-sample and particle-particle interactions. The disorder in the sphere array of course leads to considerable broadening of the spectrum. To analyze this in more detail, we display in Fig. 6 (using a photon-energy scale) the diffuse scattering intensity for three different coverages $p = 0.1$, $p = 0.2$, and $p = 0.5$, respectively. It is evident that the particles do not act independently of each other already from the fact that the scattering intensity as a function of coverage saturates for photon energies above 2 eV or so. Overall, $p = 0.2$ gives a stronger scattering than $p = 0.5$. This is in contrast with the situation at the peaks at 1.1 eV and 1.7 eV where the scattering intensity is basically proportional to p , consistent with a picture where the different particles scatter light essentially independently of each other.

While the effects of particle-particle interactions are less clean-cut in the previous case than when the particles are much smaller than $\lambda/2\pi$ (cf. Ref. 15), we can still gain some more insight into what is happening in the various parts of the “scattering band” by looking at the field distribution around the average objects at different photon energies.²⁷ Figure 7 shows the electric field around an average scatterer at 2.5 eV, 2.9 eV and 3.6 eV, when an array of such scatterers are placed on a Si/SiO₂/Si sample with $d_1 = 160$ nm and $d_2 = 200$ nm and illuminated by light at normal incidence. The solid arrows represent the real part of the field (in phase with the incident wave in the plane $z = 0$). (i) At 2.5 eV there is a concentration of the field to the region in between the particles. This is a result of direct particle-particle

interactions where a particle is polarized by the effective field which is the sum of the external field and the field from the other particles, the nearest neighbors giving the largest contributions. Indeed, if one considers two (real) silver spheres with $R = 50$ nm at a distance 120 nm from each other that are driven by an external field directed along the line joining the two spheres, they have a collective resonance at about 2.6 eV. Thus this resonance is redshifted relative to the dipole resonance of an isolated particle which occurs at about 3.1 eV if $R = 50$ nm since the field from the neighbouring sphere acts in phase with the external field when the frequency lies below the single-sphere resonance frequency. In Fig. 6 we see that as the coverage is increased, the low-frequency edge of the scattering band shifts to the left and the intensity in this part of the spectrum increases, consistent with the growing importance of particle-particle interactions at a larger p . (ii) Looking at the fields at 2.9 eV we see that they are more concentrated to the region in space near the sample. Here particle-sample interactions play a relatively important role. What happens is that the external field polarizes the particles, and the particle dipole moments, in turn, induce image charges in the sample that reinforce the driving electric field. In this way the dipole, but also higher multipole moments on the particle are further amplified, leading to the field concentration near the sample surface. (iii) At 3.6 eV, on the other hand, the fields are concentrated to the upper (vacuum) side of the particles, and the fields are also weaker in this case than in the previous ones. Here the induced dipole moment on a sphere is essentially out of phase with the driving field. Hence the image charges in the sample this time set up an induced field opposing the external electric field acting on the particle. The enhancement mechanisms discussed above are no longer efficient and the fields are localized to the top side of the particle.

In their experiments, Stuart and Hall⁵ also studied light scattering from an overlayer of Ag particles on a silver sample covered by spacer layers of LiF of varying thickness. The silver surface possesses elementary excitations in the form of surface plasmons and these excitations can mediate interactions between the silver particles in the overlayer. Also in this case, the experimental results exhibited scattering resonances, albeit very broad ones, at relatively small photon energies. In the experimental paper⁵ they were discussed along the same lines as the resonances occurring in the case of the layered Si/SiO₂/Si sample, namely as the result of strong surface-mediated particle-particle interactions that enhance the scattering intensities.

Figure 8 shows results for the calculated scattering intensity from a particle overlayer on silver samples with LiF spacer layers of two different thicknesses, 120 nm and 200 nm. With a Ag sample the calculations are numerically more difficult than with a Si sample because the surface response now, due to surface plasmons, has considerably sharper features than what one sees in Fig. 5. There is therefore some numerical noise in the results, as

can be seen as irregular oscillations of the curves in Fig. 8.

The results in Fig. 8 agree well with the experimental ones from a qualitative point of view. The shape of the spectra are the same as in the experiment, even if the positions of the maxima are somewhat shifted compared with the results in Fig. 4 of Ref. 5. Part of the explanation for this may be that the height of the particles is smaller in the experiment than in the calculation. As was the case with a Si/SiO₂/Si sample, the calculated intensity of the scattered light closely follows the strength of the driving field, which is also plotted in the figure. We can conclude that also for the silver sample the overall shape of the diffuse scattering spectrum is set by the driving electric field which in turn is affected by interference effects between waves reflected from the different interfaces in the sample. Increasing the thickness of the LiF layer from 120 nm to 200 nm shifts both the peaks in the scattering spectrum towards longer wavelengths. This brings with it a decrease in the scattering intensity at long wavelengths since the maximum of the driving field falls at longer wavelengths where the scattering cross section of the particles is smaller. The scattering intensity at the short-wavelength peak, on the other hand, increases when d increases from 120 nm to 200 nm. Both these trends for the scattering intensity are qualitatively consistent with the experimental results. The strength of the short-wavelength peak grows when d changes from 120 nm to 200 nm because the maximum of the driving field in the latter case coincides with the previously discussed resonance near 2.5 eV at which the in-plane dipole moments of neighbouring particles oscillate in phase [cf. Fig. 7 (a)].

V. SUMMARY

In this paper we have presented a formalism by which the diffuse light scattering intensity from a disordered array of spherical nanoparticles can be calculated. The theory is built on an expansion of the electromagnetic field around the nanoparticles in terms of multipoles, and takes into account interparticle interactions mediated by near and far fields as well as the sample. The theory was then applied to systems similar to those studied experimentally by Stuart and Hall⁵ in which silver nanoparticles are placed on layered substrates that support various surface waves. The results of the present calculation agrees rather well with the experimental ones. In particular the intensity of diffusely scattered light from nanoparticles on a layered Si/SiO₂/Si sample shows several characteristic peaks at long wavelengths. We have shown that these peaks are due to reflection resonances of the sample and not enhanced particle-particle interactions mediated by sample waveguide modes.

ACKNOWLEDGMENTS

This research was supported by the Swedish Natural Science Research Council (NFR) and the SSF through the Nanometer Consortium at Lund University. Discussions with P. Apell and A. Leitner are gratefully acknowledged.

APPENDIX A: COUPLING TO PLANE WAVES

1. Plane-wave-to-multipole coupling

In this Appendix we present results for the coupling factors between multipole fields and plane waves. For a detailed derivation we refer to Ref. 30.

We consider first a plane wave written on the general form,

$$\mathbf{E}(\mathbf{r}) = \left\{ E^{(s)} \hat{s} + E^{(p)} \hat{p} \right\} e^{i\mathbf{q} \cdot \mathbf{r}} \quad (\text{A1})$$

where $\hat{s} = [\hat{z} \times \hat{\mathbf{q}}_{\parallel}]$ and $\hat{p} = -[\hat{q} \times (\hat{z} \times \hat{\mathbf{q}}_{\parallel})]$ that is incident on a sphere. This wave can be expanded in terms of electric and magnetic multipoles around the center \mathbf{R}_j of sphere j as

$$\mathbf{E}(\mathbf{r}) = \sum_{lm} k a_{lm}^{(M)} j_l(kr) \mathbf{X}_{lm} + i \nabla \times \left[a_{lm}^{(E)} j_l(kr) \mathbf{X}_{lm} \right], \quad (\text{A2})$$

where $r = |\mathbf{r} - \mathbf{R}_j|$.

The coefficients in this expression depend linearly on the amplitudes of the incoming plane wave, i.e.

$$\begin{aligned} a_{lm}^{(E)} &= f_{lm}^{Ep}(\mathbf{q}) E^{(p)} + f_{lm}^{Es}(\mathbf{q}) E^{(s)}, \quad \text{and} \\ a_{lm}^{(M)} &= f_{lm}^{Mp}(\mathbf{q}) E^{(p)} + f_{lm}^{Ms}(\mathbf{q}) E^{(s)}, \end{aligned} \quad (\text{A3})$$

where

$$f_{lm}^{Ep}(\mathbf{q}) = f_{lm}^{Ms}(\mathbf{q}) = k^{-1} U_{lm}(\mathbf{q}) e^{i\mathbf{q} \cdot \mathbf{R}_j}, \quad (\text{A4})$$

and

$$f_{lm}^{Es}(\mathbf{q}) = -f_{lm}^{Mp}(\mathbf{q}) = k^{-1} V_{lm}(\mathbf{q}) e^{i\mathbf{q} \cdot \mathbf{R}_j}. \quad (\text{A5})$$

The quantities, $U_{lm}(\mathbf{q})$ and $V_{lm}(\mathbf{q})$, are given by

$$\begin{aligned} U_{lm}(\mathbf{q}) &= -\frac{2\pi i^l (-1)^m}{\sqrt{l(l+1)}} [s_+ F_+(l, m) Y_{l, -m-1}(\Omega_q) + \\ &\quad + s_- F_-(l, m) Y_{l, -m+1}(\Omega_q)], \end{aligned} \quad (\text{A6})$$

where Ω_q denotes the direction, the angles θ_q and ϕ_q , of \mathbf{q} and

$$s_{\pm} = \hat{s} \cdot \hat{x} \pm i \hat{s} \cdot \hat{y},$$

and

$$\begin{aligned} V_{lm}(\mathbf{q}) &= -\frac{2\pi i^l (-1)^m}{\sqrt{l(l+1)}} [\eta_+ F_+(l, m) Y_{l, -m-1}(\Omega_q) + \\ &\quad + \eta_- F_-(l, m) Y_{l, -m+1}(\Omega_q) - \eta_z 2m Y_{l, -m}(\Omega_q)], \end{aligned} \quad (\text{A7})$$

with

$$\hat{\eta} = k^{-1} \mathbf{q} \times (\hat{z} \times \hat{\mathbf{q}}_{\parallel}); \quad \eta_{\pm} = \eta_x \pm i\eta_y,$$

and

$$\begin{aligned} F_+(l, m) &= \sqrt{(l-m)(l+m+1)}, \quad \text{and} \\ F_-(l, m) &= \sqrt{(l+m)(l-m+1)}. \end{aligned} \quad (\text{A8})$$

The above expressions are also valid for evanescent waves that decay exponentially in the positive or negative z direction. The most general wave vector we consider here lies on the mass shell, and can be written

$$\mathbf{q} = \mathbf{q}_{\parallel} \pm \hat{z} \sqrt{k^2 - |\mathbf{q}_{\parallel}|^2}. \quad (\text{A9})$$

The plus sign holds for waves that are outgoing (propagating or evanescent) in the positive z direction, and then $\cos \theta_q$ is either real and positive, or lies on the positive imaginary axis. The minus sign holds for outgoing waves in the negative z direction.

2. Multipole-to-plane-wave coupling

We also need to know how much the outgoing waves from a multipole contributes to the amplitude of a certain plane wave. To this end we apply the Kirchoff integrals. Thus, for a magnetic multipole we calculate \mathbf{E} from Eq. (2.1), while for an electric multipole we calculate \mathbf{B} from Eq. (2.2). To carry out the integration we use the following form for the Green's function

$$G(\mathbf{r}, \mathbf{r}') = i \int \frac{d^2 q_{\parallel}}{(2\pi)^2} \frac{e^{i\sqrt{k^2 - q_{\parallel}^2} |z - z'|}}{2\sqrt{k^2 - q_{\parallel}^2}} e^{i\mathbf{q}_{\parallel} \cdot (\mathbf{r}_{\parallel} - \mathbf{r}'_{\parallel})}. \quad (\text{A10})$$

The scalar plane wave appearing here is expanded in terms of spherical harmonics, so that the overlap integrals with the multipole fields can be carried out. As is evident from Eq. (A10), the radiated field is a linear combination of many plane waves, and the result can be written as

$$\mathbf{E}(\mathbf{r}) = \sum_{lm, \sigma} a_{lm, \sigma}^{\sigma} \int \frac{d^2 q_{\parallel}}{(2\pi)^2} [g_{lm}^{s\sigma}(\mathbf{q}) \hat{s} + g_{lm}^{p\sigma}(\mathbf{q}) \hat{p}] e^{i\mathbf{q} \cdot \mathbf{r}}. \quad (\text{A11})$$

The coupling factors are found to be

$$g_{lm}^{pE}(\mathbf{q}) = g_{lm}^{sM}(\mathbf{q}) = \frac{e^{-i\mathbf{q} \cdot \mathbf{R}_j}}{2\sqrt{k^2 - |\mathbf{q}_{\parallel}|^2}} (-1)^{l+m+1} U_{l, -m}(\mathbf{q}), \quad (\text{A12})$$

and

$$g_{lm}^{sE}(\mathbf{q}) = -g_{lm}^{pM}(\mathbf{q}) = \frac{(-1)^{l+m+1} e^{-i\mathbf{q}\cdot\mathbf{R}_j}}{2\sqrt{k^2 - |\mathbf{q}_\parallel|^2}} V_{l,-m}(\mathbf{q}). \quad (\text{A13})$$

APPENDIX B: CALCULATION OF INTERPARTICLE COUPLING

The Fourier transform of $\overset{\leftrightarrow}{t}^{\text{dir}}$ is given by

$$\overset{\leftrightarrow}{t}_{\mathbf{Q}}^{\text{dir}} = \sum_{j \neq i} \overset{\leftrightarrow}{t}_{ij}^{\text{dir}} e^{-i\mathbf{Q}\cdot(\mathbf{R}_i - \mathbf{R}_j)} \quad (\text{B1})$$

where i can be any site. If all spheres in the array sends out waves described by $\vec{b} e^{i\mathbf{Q}\cdot\mathbf{R}_j}$, the waves received at site i (without any intermediate scattering taking place) is

$$\begin{aligned} \vec{a}_i &= \sum_{j \neq i} \overset{\leftrightarrow}{t}_{ij}^{\text{dir}} e^{i\mathbf{Q}\cdot\mathbf{R}_j} \vec{b} = e^{i\mathbf{Q}\cdot\mathbf{R}_i} \sum_{j \neq i} \overset{\leftrightarrow}{t}_{ij}^{\text{dir}} e^{-i\mathbf{Q}\cdot(\mathbf{R}_i - \mathbf{R}_j)} \vec{b} = \\ &= e^{i\mathbf{Q}\cdot\mathbf{R}_i} \overset{\leftrightarrow}{t}_{\mathbf{Q}}^{\text{dir}} \vec{b}. \end{aligned} \quad (\text{B2})$$

In particular, at the site at the origin,

$$\vec{a}_0 = \overset{\leftrightarrow}{t}_{\mathbf{Q}}^{\text{dir}} \vec{b}.$$

We therefore calculate $\overset{\leftrightarrow}{t}_{\mathbf{Q}}^{\text{dir}}$ by identifying the waves incident on the sphere at the origin.

We can simplify the detailed calculation by realizing that outside a source sphere the outgoing waves appears to originate from the center of the sphere, and likewise, when expanding the waves incident on the sphere at the origin in different multipoles, this can be done at any distance from the sphere center. In the calculations at hand here we therefore set the radius of the source sphere to r_2 and that of the receiving sphere to r_1 and let both these radii tend to zero. The physical size (the radius R) of the real spheres is of course relevant to the physics, but this enters the calculation only through the response functions $s_l^{(E)}$ and $s_l^{(M)}$.

Consider now an electric multipole source with angular momentum quantum numbers l' and m' . We calculate the \mathbf{B} field this generates near the origin using the Kirchoff integral in Eq. (2.2), where now the last term vanishes, so that

$$\begin{aligned} \mathbf{B}(\mathbf{r}_1) &= \sum_{j \neq 0} r_2^2 \int d\Omega_2 \left[-\frac{ik}{c} (\hat{r}_2 \times \mathbf{E}(\mathbf{r}_2)) G(\mathbf{r}_1, \mathbf{r}_2 - \mathbf{R}_j) \right. \\ &\quad \left. + (\hat{r}_2 \times \mathbf{B}(\mathbf{r}_2)) \nabla_2 G(\mathbf{r}_1, \mathbf{r}_2 - \mathbf{R}_j) \right] e^{i\mathbf{Q}\cdot\mathbf{R}_j}. \end{aligned} \quad (\text{B3})$$

Here the phase factor $e^{i\mathbf{Q}\cdot\mathbf{R}_j}$ has been included explicitly, and $\mathbf{B}(\mathbf{r}_2)$ and $\mathbf{E}(\mathbf{r}_2)$ should be evaluated on the sphere at the origin (even if this, due to the condition $j \neq 0$, does not contribute to the sum).

The summation over lattice sites only involves the Green's function and the last phase factor, two scalar quantities. We therefore change the order between integration and summation and begin by evaluating the lattice sum

$$\begin{aligned} S_{\mathbf{Q}} &= \sum_{j \neq 0} G(\mathbf{r}_1, \mathbf{r}_2 - \mathbf{R}_j) e^{i\mathbf{Q}\cdot\mathbf{R}_j} = \\ &= \sum_{j \neq 0} \frac{\exp[ik|\mathbf{r}_1 - \mathbf{r}_2 - \mathbf{R}_j|]}{4\pi|\mathbf{r}_1 - \mathbf{r}_2 - \mathbf{R}_j|} e^{i\mathbf{Q}\cdot\mathbf{R}_j} \end{aligned} \quad (\text{B4})$$

and its gradient $\nabla_2 S_{\mathbf{Q}}$. The calculation uses Ewald methods borrowed from KKR theory.³¹ The sum can be expressed both in terms of a one-center expansion

$$S_{\mathbf{Q}} = \sum_{L=0}^{\infty} \sum_{M=-L}^L D_{LM} j_L(kr_{12}) Y_{LM}(\Omega_{12}), \quad (\text{B5})$$

where r_{12} and Ω_{12} denote the length and direction of the vector $\mathbf{r}_{12} = \mathbf{r}_1 - \mathbf{r}_2$, and a two-center expansion

$$S_{\mathbf{Q}} = \sum_{lm'l'm'} A_{lm'l'm'} j_l(kr_1) j_{l'}(kr_2) Y_{lm}(\Omega_1) Y_{l'm'}^*(\Omega_2). \quad (\text{B6})$$

The two sets of expansion coefficients are related through

$$A_{lm'l'm'} = 4\pi i^{l'-l} \sum_{LM} i^L D_{LM} C_{lm'l'm'}^{LM}, \quad (\text{B7})$$

where $C_{lm'l'm'}^{LM}$ denotes a Gaunt integral

$$C_{lm'l'm'}^{LM} = \int d\Omega Y_{lm}^*(\Omega) Y_{LM}(\Omega) Y_{l'm'}(\Omega). \quad (\text{B8})$$

The two expansions serve different purposes. When evaluating \mathbf{B} from Eq. (B3), and then projecting the result onto different multipoles at the origin, we will use the two-center expansion. The one-center expansion is useful because using Ewald methods $S_{\mathbf{Q}}$ can be split into a long-range part and a short-range part, and the coefficients D_{LM} can be calculated rapidly.

There are three contributions to D_{LM} ,

$$D_{LM} = D_{LM}^{(1)} + D_{LM}^{(2)} + D_{00}^{(3)} \delta_{L0}. \quad (\text{B9})$$

The long-range contribution $D_{LM}^{(1)}$ can be expressed as a sum of crystal-rod integrals

$$\begin{aligned} D_{LM}^{(1)} &= \frac{4\pi i^L}{A_{\text{cell}} k^L} \sum_{\mathbf{G}} \int \frac{dq_z}{2\pi} \\ &\quad \times \frac{|\mathbf{q} + \mathbf{G}|^L}{|\mathbf{q} + \mathbf{G}|^2 - k^2} Y_{LM}^*(\Omega_{\mathbf{q}+\mathbf{G}}) e^{(k^2 - |\mathbf{q}+\mathbf{G}|^2)/\eta}, \end{aligned} \quad (\text{B10})$$

here $\mathbf{q} = \mathbf{Q} + \hat{z}q_z$ and η is a separation parameter. $D_{LM}^{(2)}$ comes from a direct summation over the lattice, and thus collects short-range interactions

$$D_{LM}^{(2)} = \frac{2^{L+1}}{\sqrt{\pi} k^L} \sum_{j \neq 0} |\mathbf{R}_j|^L e^{i\mathbf{Q} \cdot \mathbf{R}_j} Y_{LM}^*(\Omega_{\mathbf{R}_j}) I_L(|\mathbf{R}_j|, k) \quad (\text{B11})$$

where the integral

$$I_L(|\mathbf{R}_j|, k) = \int_{\sqrt{\eta}/2}^{\infty} d\xi \xi^{2L} \exp[-\xi^2 |\mathbf{R}_j|^2 + k^2/4\xi^2] \quad (\text{B12})$$

can be related to the complementary error function. The last contribution compensates for the fact that $D_{00}^{(1)}$ contains some self-interaction contributions,

$$D_{00}^{(3)} = -\frac{ik}{\sqrt{4\pi}} + \frac{\sqrt{\eta}}{2\pi} \sum_{n=0}^{\infty} \frac{(k^2/\eta)^n}{n!(2n-1)}. \quad (\text{B13})$$

In the calculations here the separation parameter η was related to the lattice parameter a as $\eta = 3.24/a^2$; the value of η of course does not affect the result for D_{LM} .

To proceed with the calculation of $\vec{t}_{\mathbf{Q}}$, we insert the two-center expansion Eq. (B6) into Eq. (B3), together with expressions for $\hat{r}_2 \times \mathbf{E}$ and $\hat{r}_2 \times \mathbf{B}$ for a certain electric multipole ($L'M'$). The resulting surface integrations are now straightforward since $\mathbf{X}_{L'M'}$ is a linear combination of $Y_{L',M'+1}$, $Y_{L',M'}$, and $Y_{L',M'-1}$. We get

$$\begin{aligned} \mathbf{B}(\mathbf{r}_1) = & -\frac{i}{c} \frac{b_{L'M'}^{(E)}}{2\sqrt{L'(L'+1)}} \sum_{lm} j_l(kr_1) Y_{lm}(\Omega_1) \\ & \times \{ \hat{n}_- F_+(L', M') A_{l,m,L',M'+1} \\ & + \hat{n}_+ F_-(L', M') A_{l,m,L',M'-1} + \hat{n}_z 2M' A_{l,m,L',M'} \}. \end{aligned} \quad (\text{B14})$$

In this expression $\hat{n}_{\pm} = \hat{x} \pm i\hat{y}$, $\hat{n}_z = \hat{z}$, and F_+ and F_- are defined in Eq. (A8).

Next we project \mathbf{B} onto different multipoles around the origin. The field corresponding to an electric multipole (LM) can be written

$$\mathbf{B} = \frac{k}{c} a_{LM}^{(E)} j_L(kr_1) \mathbf{X}_{LM}(\Omega_1),$$

therefore

$$\frac{k}{c} a_{LM}^{(E)} j_L(kr_1) = \int d\Omega_1 (\mathbf{X}_{LM}(\Omega_1))^* \cdot \mathbf{B}(\mathbf{r}_1), \quad (\text{B15})$$

and the final result for $t_{LML'M'}^{(EE)} = a_{LM}^{(E)}/b_{L'M'}^{(E)}$ reads

$$\begin{aligned} t_{LML'M'}^{(EE)} = & -\frac{i}{2k} \frac{1}{\sqrt{L(L+1)L'(L'+1)}} \\ & \times \{ F_+(L, M) F_+(L', M') A_{L,M+1,L',M'+1} \\ & + F_-(L, M) F_-(L', M') A_{L,M-1,L',M'-1} \\ & + 2MM' A_{L,M,L',M'} \}. \end{aligned} \quad (\text{B16})$$

The corresponding calculation for the projection onto a magnetic multipole (LM) is somewhat more involved. We use the fact that for a magnetic multipole

$$\mathbf{r}_1 \cdot \mathbf{B}(\mathbf{r}_1) = \frac{1}{c} a_{LM}^{(M)} j_L(kr_1) \sqrt{L(L+1)} Y_{LM}(\Omega_1),$$

and consequently

$$\frac{1}{c} a_{LM}^{(M)} j_L(kr_1) \sqrt{L(L+1)} = \int d\Omega_1 Y_{LM}^*(\Omega_1) [\mathbf{r}_1 \cdot \mathbf{B}]. \quad (\text{B17})$$

Here the Cartesian components of \mathbf{r}_1 introduce spherical harmonics Y_{11} , Y_{10} , and Y_{1-1} into the integral. The final result thus contains Gaunt integrals,

$$\begin{aligned} t_{LML'M'}^{(ME)} = & -\frac{i}{2k} \frac{2L+1}{\sqrt{L(L+1)L'(L'+1)}} \sqrt{\frac{4\pi}{3}} \\ & \times \left\{ \sqrt{2} C_{LM,L-1,M+1}^{1,-1} F_+(L', M') A_{L-1,M+1,L',M'+1} \right. \\ & - \sqrt{2} C_{LM,L-1,M-1}^{1,1} F_-(L', M') A_{L-1,M-1,L',M'-1} \\ & \left. + C_{LM,L-1,M}^{1,0} 2M' A_{L-1,M,L',M'} \right\}. \end{aligned} \quad (\text{B18})$$

We have determined half of the elements in $\vec{t}_{\mathbf{Q}}$. If the sources instead are magnetic multipoles we use the other Kirchoff integral in Eq. (2.1) to calculate $\mathbf{E}(\mathbf{r}_1)$ around the origin. The calculations are perfectly analogous to the ones above and in the end one finds the following symmetry of $\vec{t}_{\mathbf{Q}}$,

$$\begin{aligned} t_{LML'M'}^{(MM)} = & t_{LML'M'}^{(EE)} \quad \text{and} \\ t_{LML'M'}^{(EM)} = & -t_{LML'M'}^{(ME)}. \end{aligned} \quad (\text{B19})$$

APPENDIX C: CALCULATION OF SAMPLE-MEDIATED INTERACTIONS

Here we will calculate the sample-mediated self-interaction \vec{w} as well as $\vec{t}_{\mathbf{Q}}^{\text{sub}}$.

Starting with \vec{w} , suppose a certain multipole ($l'm'\sigma'$) is excited on a sphere. Then plane waves are sent out from the sphere, reflected off the sample surface either as s or p polarized light, and after that the wave impinges on the sphere again. The strength a_{lm}^{σ} of the incident wave can be calculated using the previously introduced functions f and g , and the result reads

$$\begin{aligned} w_{lm'l'm'}^{\sigma\sigma'} = & \sum_{\sigma''} \int \frac{d^2 q_{\parallel}}{(2\pi)^2} \\ & \times f_{lm}^{\sigma\sigma''}(\mathbf{q}_+) \chi_{\sigma''}(\mathbf{q}_{\parallel}) g_{l'm'}^{\sigma''\sigma'}(\mathbf{q}_-) e^{2i\sqrt{k^2 - q_{\parallel}^2} |z_0|}, \end{aligned} \quad (\text{C1})$$

where

$$\mathbf{q}_{\pm} = \mathbf{q}_{\parallel} \pm \hat{z} \sqrt{k^2 - |\mathbf{q}_{\parallel}|^2}$$

and σ'' denotes the plane-wave polarization (s or p). The angular integration (over the different directions of \mathbf{q}_{\parallel}) is straightforward, and yields a finite result only when $m = m'$. The remaining integration over $|\mathbf{q}_{\parallel}|$ must be done numerically.

Once \vec{w} is known, it is relatively easy to calculate $\vec{t}_{\mathbf{Q}}^{\text{sub}}$. If the same multipole is excited on all the spheres, with relative phase $e^{i\mathbf{Q}\cdot\mathbf{R}_j}$, the incident wave at the origin must be proportional to a sum of $\vec{t}_{\mathbf{Q}}^{\text{sub}}$ and \vec{w} . This sum is easily calculated thanks to the periodicity of the radiating system. A certain tensor element is found through a summation over the 2D reciprocal lattice

$$t_{lm'l'm',\mathbf{Q}}^{\text{sub},\sigma\sigma'} + w_{lm'l'm'}^{\sigma\sigma'} = \frac{1}{A_{\text{cell}}} \sum_{\sigma''} \sum_{\mathbf{G}} \times f_{lm}^{\sigma\sigma''}(\mathbf{q}_+) \chi_{\sigma''}(\mathbf{q}_{\parallel}) g_{l'm'}^{\sigma''\sigma'}(\mathbf{q}_-) e^{2i\sqrt{k^2 - q_{\parallel}^2}|z_0|}, \quad (\text{C2})$$

where now

$$\mathbf{q}_{\parallel} = \mathbf{Q} + \mathbf{G}, \quad \text{and} \quad \mathbf{q}_{\pm} = \mathbf{q}_{\parallel} \pm \hat{z}\sqrt{k^2 - |\mathbf{q}_{\parallel}|^2}.$$

-
- ¹ S. Nie and S. R. Emory, *Science* **275**, 1102 (1997); K. Kneipp *et al.*, *Phys. Rev. Lett.* **78**, 1667 (1997); H. Xu, E. J. Bjerneld, M. Käll, and L. Börjesson, *ibid.* **83**, 4357 (1999).
- ² R. Berndt, J. K. Gimzewski, and P. Johansson, *Phys. Rev. Lett.* **67**, 3796 (1991); **71**, 3493 (1993).
- ³ T. W. Ebbesen, H. J. Lezec, H. F. Ghaemi, T. Thio, and P. A. Wolff, *Nature* **391**, 667 (1998); M. B. Sobnack, W. C. Tan, N. P. Wanstall, T. W. Priest and J. R. Sambles, *Phys. Rev. Lett.* **80**, 5667 (1998); T. López-Rios, D. Mendoza, F. J. Garcia-Vidal, J. Sanchez-Dehesa, and B. Pannetier, *ibid.* **81**, 665 (1998).
- ⁴ J. A. Porto, F. J. Garcia-Vidal, and J. B. Pendry, *Phys. Rev. Lett.* **83**, 2845 (1999); L. Salomon, F. Grillot, A. V. Zayats, and F. de Fournel, *ibid.* **86**, 1110 (2001); L. Martin-Moreno, F. J. Garcia-Vidal, H. J. Lezec, K. M. Pellerin, T. Thio, J. B. Pendry, and T. W. Ebbesen, *ibid.* **86**, 1114 (2001).
- ⁵ H. R. Stuart and D. G. Hall, *Phys. Rev. Lett.* **80**, 5663 (1998); *Appl. Phys. Lett.* **73**, 3815 (1998).
- ⁶ B. Lamprecht, G. Schider, R. T. Lechner, H. Ditlbacher, J. R. Krenn, A. Leitner, and F. R. Aussenegg, *Phys. Rev. Lett.* **84**, 4721 (2000).
- ⁷ S. Linden, J. Kuhl, and H. Giessen, *Phys. Rev. Lett.* **86**, 4688 (2001).

- ⁸ J. M. Gérard, B. Sermage, B. Gayral, B. Legrand, E. Costard, and V. Thierry-Mieg *Phys. Rev. Lett.* **81**, 1110 (1998). M. Hopmeier, W. Guss, M. Deussen, E. O. Göbel, and R. F. Mahrt, *ibid.* **82**, 4118 (1999); M. Bayer, T. L. Reinecke, F. Weidner, A. Larionov, A. McDonald, and A. Forchel, *ibid.* **86**, 3168 (2001).
- ⁹ M. L. Brongersma, J. W. Hartman, and H. A. Atwater, *Phys. Rev. B* **62**, R16 356 (2000).
- ¹⁰ T. Yamaguchi, S. Yoshida, and A. Kinbara, *Thin Solid Films* **21**, 173 (1974).
- ¹¹ W. R. Holland and D. G. Hall, *Phys. Rev. Lett.* **52**, 1041 (1984).
- ¹² A. Leitner, Z. Zhao, H. Brunner, F. R. Aussenegg, and A. Wokaun, *Appl. Optics* **32**, 102 (1993).
- ¹³ K. Ohtaka, *Phys. Rev. B* **19**, 5057 (1979); H. Miyazaki and K. Ohtaka, *ibid.*, **58**, 6920 (1998).
- ¹⁴ W. Lamb, D. Wood, and N. W. Ashcroft, *Phys. Rev. B* **21**, 2248 (1980).
- ¹⁵ B. N. J. Persson and A. Liebsch, *Phys. Rev. B* **28**, 4247 (1983).
- ¹⁶ M. Meier, A. Wokaun, and P. F. Liao, *J. Opt. Soc. Am. B* **2**, 931 (1985).
- ¹⁷ P. A. Bobbert and J. Vlieger, *Physica* **137A**, 209 (1986); P. A. Bobbert, J. Vlieger, and R. Greef, *ibid.* **137A**, 243 (1986).
- ¹⁸ R. Fuchs and F. Claro, *Phys. Rev. B* **39**, 3875 (1989).
- ¹⁹ N. Stefanou and A. Modinos, *J. Phys.: Condens. Matter* **3**, 8149 (1991).
- ²⁰ F. J. Garcia de Abajo, *Phys. Rev. B* **60**, 6086 (1999).
- ²¹ S. C. Kitson, W. L. Barnes, and J. R. Sambles, *Phys. Rev. Lett.* **77**, 2670 (1996).
- ²² S. I. Bozhevolnyi, J. Erland, K. Leosson, P. M. W. Skovgaard, and J. M. Hvam, *Phys. Rev. Lett.* **86**, 3008 (2001).
- ²³ G. Rickayzen, *Green's Functions and Condensed Matter*, (Academic Press, London, 1980), pp. 285–311.
- ²⁴ G. D. Mahan, *Many-Particle Physics* (Pergamon, New York, 1990), Chapter 7.
- ²⁵ E. D. Palik, *Handbook of Optical Constants of Solids*, (Academic Press, New York, 1985).
- ²⁶ J. D. Jackson, *Classical Electrodynamics*, (Wiley, New York, 1999).
- ²⁷ In the numerical calculations we used $l_{max} = 3$. This is sufficient to obtain convergence for the scattered intensity. However, the results for the fields near a particle presented in Fig. 7 would change to a certain extent if more multipoles were included.
- ²⁸ J. Zak, E. R. Moog, C. Liu, and S. D. Bader, *Phys. Rev. B* **43**, 6423 (1991); **46**, 5883 (E) (1992).
- ²⁹ In the experiment the peaks occur at about 780 nm and 1250 nm. The sample used there had also a 30 nm thick LiF top layer.
- ³⁰ P. Johansson, S. P. Apell, and D. R. Penn, to appear in *Phys. Rev. B* (1 July 2001). [See preprint at xxx.lanl.gov/abs/cond-mat/0102226.]
- ³¹ F. S. Ham and B. Segall, *Phys. Rev.* **124**, 1786 (1961).

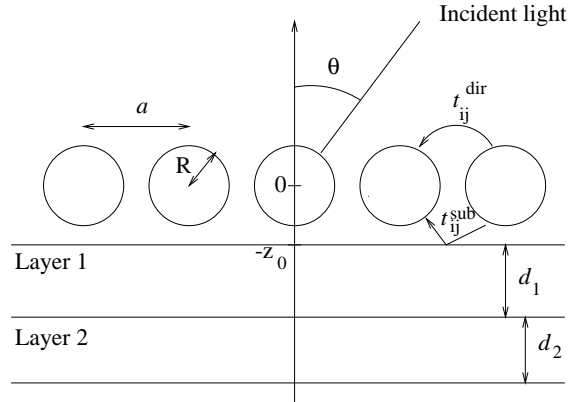
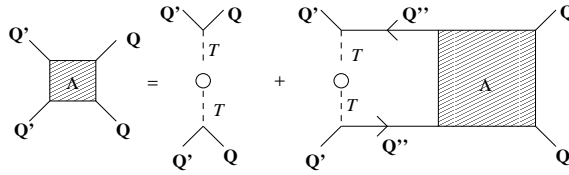


FIG. 1. Schematic illustration of the sample and overlayer of spheres. The two sample layers have thicknesses d_1 and d_2 , respectively. A lattice (lattice gas) of spherical particles with radius R and lattice parameter a covers the sample. The particles interact through direct t_{ij}^{dir} and sample-mediated t_{ij}^{sub} interactions. (The empty space between the particle layer and the sample is there only for illustrative purposes; the particles do rest on the sample.)



Johansson, FIG. 2

FIG. 2. Diagrammatic representation of the Bethe-Salpeter equation illustrating how the vertex function corresponding to the diffuse scattering intensity is built up by contributions from a single scattering event (first term) as well as by contributions from repeated scattering events.

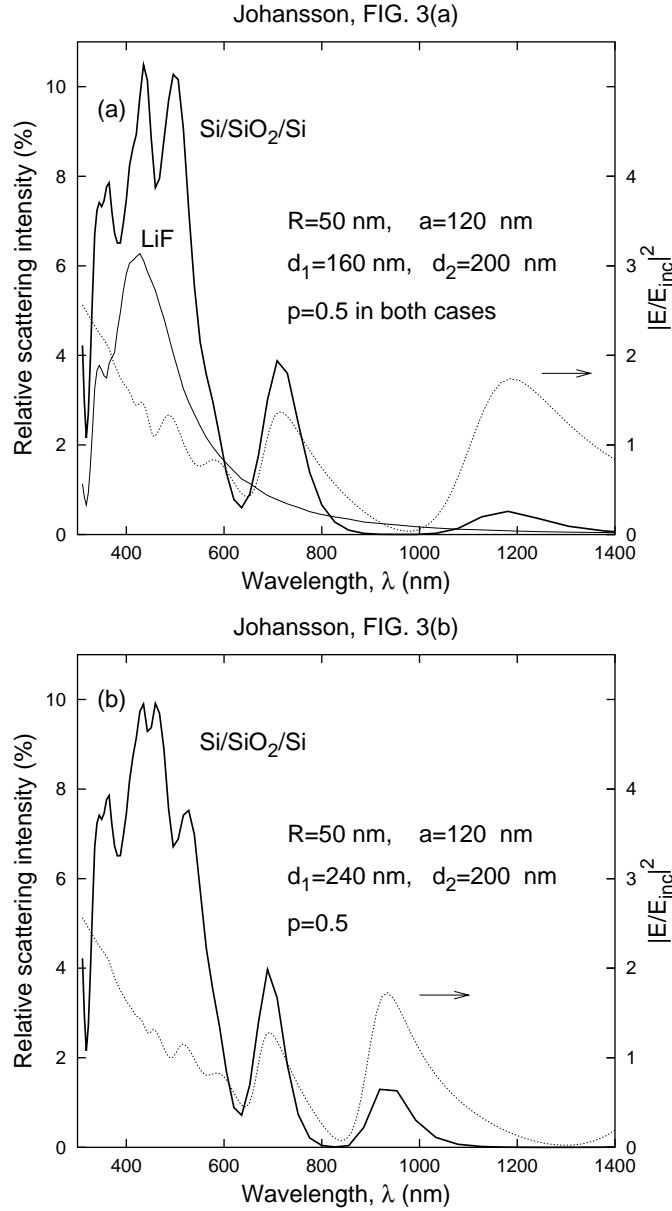


FIG. 3. (a) Relative intensity of the diffusely *reflected* light (integrated over the full solid angle 2π) from a disordered overlayer of Ag spheres. The sample is illuminated at normal incidence. The two solid curves show results obtained with a layered Si/SiO₂/Si sample and with a homogeneous LiF sample, respectively. The dotted curve shows the magnitude (squared) of the driving electric field relative to the incident field in the plane of the sphere centers. This field was calculated in the presence of the Si/SiO₂/Si sample, but without the Ag particles. (b) The corresponding results obtained with an increased thickness of the top Si layer. The maxima in the driving field have shifted to larger λ [the 1200-nm-peak from (a) falls outside the figure at ≈ 1600 nm] and the scattering-intensity maxima follow.

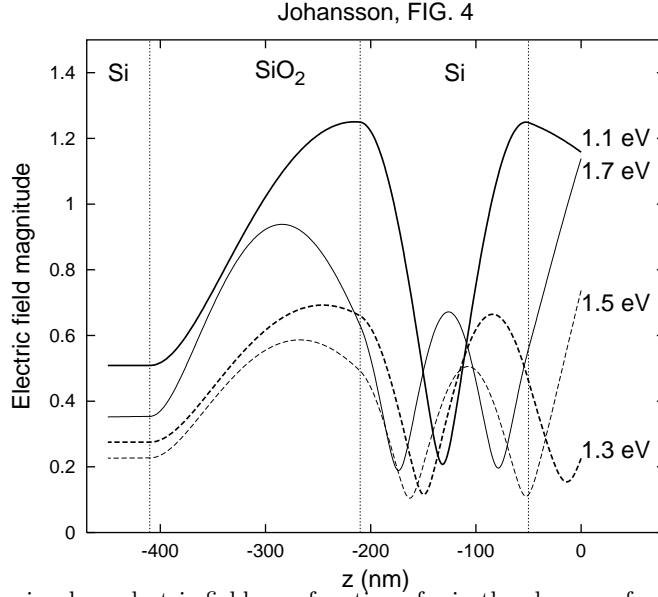


FIG. 4. The magnitude of the in-plane electric field as a function of z in the absence of any particle overlayer when a wave with amplitude 1 impinges at normal incidence on a Si/SiO₂/Si sample with the same geometric parameters as in Fig. 3 (a). Results are shown for four different photon energies as indicated next to the curves. The corresponding free-space wavelengths are 1130 nm, 950 nm, 825 nm, and 730 nm, respectively. Note that the value of the field magnitude at $z = 0$, the sphere center, equals the driving field whose square is plotted in Fig. 3 (a).

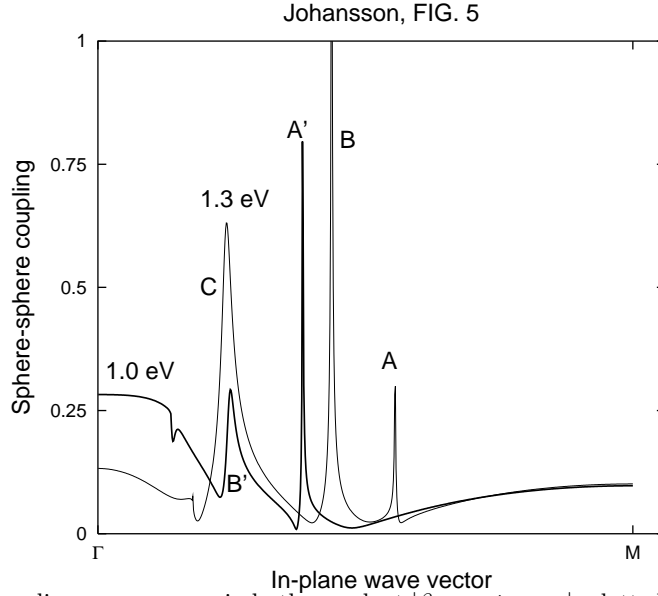


FIG. 5. The sphere-sphere coupling, or more precisely the product $|\beta_{11,11\mathbf{Q}}t_{11,11\mathbf{Q}}|$, plotted for two different photon energies 1 eV (thick curve) and 1.3 eV (thin curve) as a function of the in-plane wave vector \mathbf{Q} along the diagonal of the Brillouin zone from the center point (Γ) where $\mathbf{Q} = 0$ to the corner point (M) where $\mathbf{Q} = (2\pi/a)(\hat{x} + \hat{y})$. The peaks marked A and A' are due to s polarized waveguide modes the ones marked B and B' are due to p polarized waveguide modes. The curves exhibit discontinuities (coming from the interaction t) at the point where $|\mathbf{Q}| = k$.

Johansson, FIG. 6

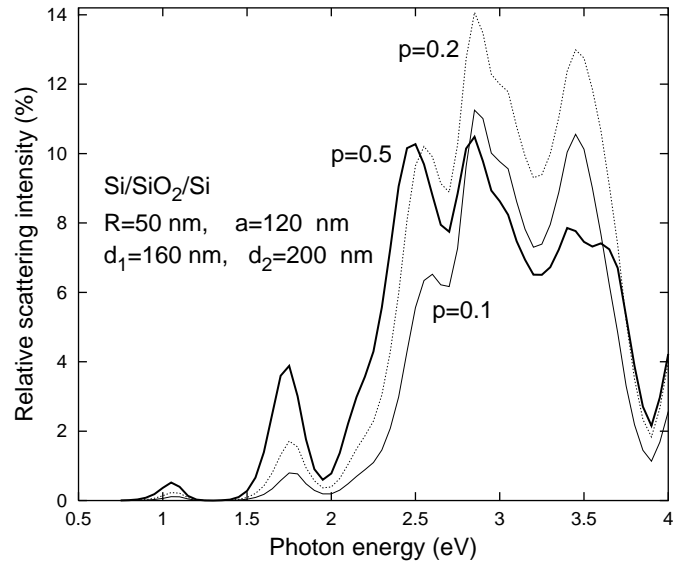
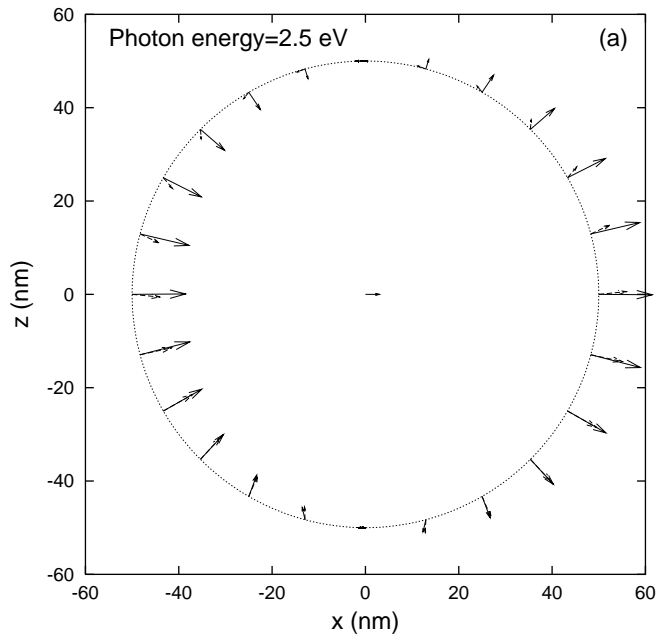


FIG. 6. Diffusely reflected light intensity from a Si/SiO₂/Si sample when the coverage p of Ag spheres is varied as indicated next to the curves. The other parameter values are the same as in Fig. 3 (a).

Johansson, FIG. 7(a)



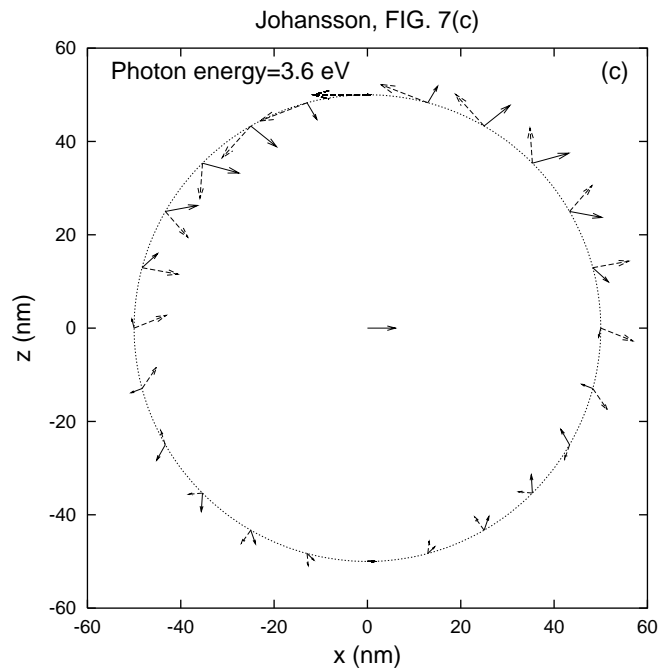
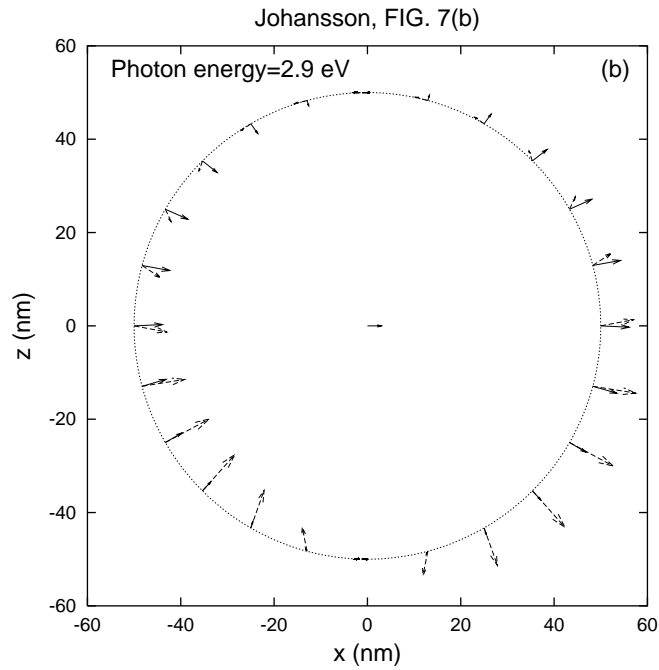


FIG. 7. The fields around an average scatterer for three different photon energies: (a) 2.5 eV, (b) 2.9 eV, and (c) 3.6 eV. The parameter values are the same as in Fig. 3 (a). The full arrows give the real part of the field (in phase with the incident wave) and the broken arrows the imaginary part. The arrow in the middle of each figure shows the strength of the field of the incident wave [thus, the scaling used in panel (c) differs from that of the other panels].

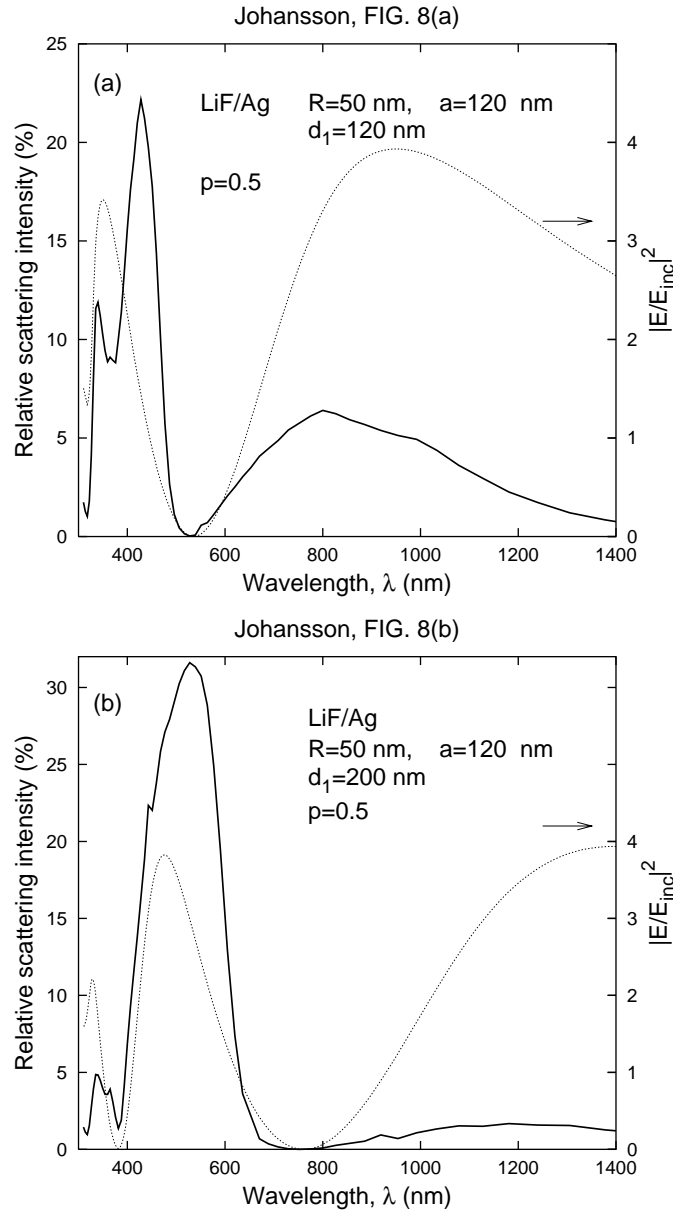


FIG. 8. Relative intensity of the diffusely *reflected* light (integrated over the full solid angle 2π) from a disordered overlayer of Ag spheres with a relative coverage $p = 0.5$ on a LiF/Ag sample. In both plots the full curves show the scattering intensity, whereas the dotted curves show the result for the (squared) driving field. The thickness of the LiF layer is (a) 120 nm and (b) 200 nm, respectively, in the two plots.